DALTON
FULL PAPER

Synthesis and magnetostructural characterization of two ferromagnetic nickel(II) dimers

M. Gotzone Barandika,[a,b] Roberto Cortés,[a] Luis Lezama,[b] M. Karmele Urtiaga,[c] M. Isabel Arriortua[c] and Teófilo Rojo *[b]

[a] *Departamento de Química Inorgánica, Facultad de Farmacia, Universidad del País Vasco, Apdo. 450, Vitoria 01080, Spain*
[b] *Departamento de Química Inorgánica, Facultad de Ciencias, Universidad del País Vasco, Apdo. 644, Bilbao 48080, Spain. E-mail: qiproapt@lg.ehu.es*
[c] *Departamento de Mineralogía-Petrología, Facultad de Ciencias, Universidad del País Vasco, Apdo. 644, Bilbao 48080, Spain*

Received 5th May 1999, Accepted 9th July 1999

Two new ferromagnetic, end-on azide-bridged nickel(II)-dimers $[\{Ni(terpy)(N_3)_2\}_2]\cdot H_2O$ **1** and $[Ni_2(terpy)_2(N_3)_3(H_2O)]ClO_4\cdot H_2O$ **2** (terpy = 2,2′ : 6′,2″-terpyridine) have been synthesized and magnetostructurally characterized through X-Ray single crystal analysis, IR spectroscopy and magnetic susceptibility measurements. The values of the Ni–N–Ni bridge angle and the magnetic coupling constant, J, are 101.6° and 22.8 cm^{-1}, respectively, for **1** and 102.5° and 13.6 cm^{-1}, respectively, for **2**. The influence of the Ni–N–Ni bridge angle on the magnetic performance of end-on azide-bridged nickel(II) dimers has been studied by means of extended Hückel molecular orbital calculations. The results indicate that the antiferromagnetic contribution of the global coupling constant decreases for increasing bridge angle between 83 and 115°.

Introduction

A perspective on the literature about the great number of works carried out in recent years on azide-containing complexes reveals that this pseudohalide ligand is undoubtedly one of the most interesting found so far in molecular magnetism.[1–10] Thus, the distinct possibilities of magnetic coupling through azide bridges arise because of the versatility of co-ordination exhibited by this ligand. In this sense, it must be pointed out that special attention has been focused on end-on azide-bridged compounds since the magnetic coupling through this type of ligand has been observed to be ferromagnetic.[1,3b,4a–d,5,6]

During the last years a great effort has been made in order to explain ferromagnetic couplings through end-on azide bridges (μ-(1,1)-N_3). Thus, there have been two major proposals about the mechanism which gives rise to ferromagnetic coupling. According to the first,[5c] the crossover between ferro- and antiferro-magnetic couplings is related to an "accidental orthogonality"[11] which involves a spin delocalization mechanism. Since the structural parameter associated with this "accidental orthogonality" is the bridge angle, the magnetic behaviour should be angle dependent. The second interpretation[2,12,13] is based on a spin polarization mechanism which implies that the electron of the bridging nitrogen atom (α spin) is partially delocalized towards the two metal orbitals. As a result, each unpaired electron of the two metal ions is likely to have a β spin, favouring ferromagnetic interactions irrespective of the bridge angle.

Most of the theoretical approaches concern simple architectures such as dimers among which those of dibridged Cu^{II} have been particularly studied. In this respect, Thompson and co-workers[5] experimentally confirmed the angle dependence of the crossover between ferro- and antiferro-magnetic couplings for a variety of copper(II) dimers. This conclusion seems to be in disagreement with the spin polarization model as it presumes a non-angle dependence of the magnetic behaviour. However, according to a recent study by Kahn and co-workers[10] based on experimentally obtained spin density maps for a particular copper(II) dimer exhibiting di-μ-N_3 bridges, neither of the mechanisms cited above is completely satisfactory but both are co-operative. Thus, the authors propose that a spin delocalization takes place from copper(II) ions toward the azido bridges followed by a spin polarization over the π orbitals of the azido groups. Alvarez and co-workers,[14] after some theoretical calculations, agree with this co-operative mechanism.

Another aspect to be taken into consideration is the influence of the energy gap (Δ) between SOMOs (Singly Occupied Molecular Orbitals) on the exchange constant. In relation to this, Alvarez and co-workers[14] have found a parabolic relationship between J and Δ^2 for copper(II) dimers exhibiting di-μ-(1,1)-N_3 bridges. Additionally, these authors have calculated that the crossover between ferro- and antiferro-magnetic coupling occurs at a bridge angle of 104° which is in good agreement with the experimental value (108°) proposed by Thompson *et al.*[5b]

The above mentioned aspects not only show the relevance of the subject but clearly suggest the importance of extending these theoretical approaches to other simple metallic systems. In relation to di-μ-(1,1)-N_3-bridged nickel(II) dimers, it is worth mentioning that all the compounds characterized so far are ferromagnetic and exhibit a narrow range of bridge angles. The complexity in the study of these systems lies not only in the presence of a second unpaired electron but also in the fact that the number of compounds characterized so far is remarkably low.

Thus, taking advantage of our experience on azide systems,[3] we have synthesized and magnetostructurally characterized two new nickel(II) dimers $[\{Ni(terpy)(N_3)_2\}_2]\cdot H_2O$ **1** and $[Ni_2(terpy)_2(N_3)_3(H_2O)]ClO_4\cdot H_2O$ **2** (terpy = 2,2′ : 6′,2″-terpyridine) as additional examples of ferromagnetic di-μ-(1,1)-N_3 bridged complexes. Furthermore, we have studied the influence of the energy gap between SOMOs on the exchange constant J, the results being compared to others in the literature.

Experimental

Synthesis

The complex $[\{Ni(terpy)(N_3)_2\}_2]\cdot H_2O$ **1** was synthesized as a green precipitate after a 4 h reflux of $[Ni(terpy)Cl(H_2O)_2]Cl\cdot H_2O$ (0.4 mmol) and NaN_3 (2.4 mmol) in MeOH–EtOH (1:1) (50 ml). The $[Ni(terpy)Cl(H_2O)_2]Cl\cdot H_2O$ complex was prepared following the procedure described elsewhere.[15] Recrystallization of the precipitate was carried out in MeOH–water (1:1) giving rise to prismatic crystals suitable for X-ray analysis.

Synthesis of $[Ni_2(terpy)_2(N_3)_3(H_2O)]ClO_4\cdot H_2O$ **2** was carried out by treating a MeOH–water (1:1) solution (50 ml) of $[\{Ni(terpy)(N_3)_2\}_2]\cdot H_2O$ **1** (0.2 mmol) with an aqueous solution of $NaClO_4$ (1.0 mmol) (25 ml). The resulting solution was left to stand at room temperature. After several days, prismatic, green, X-ray quality single crystals were obtained. Elemental analysis and atomic absorption results were in good agreement with $Ni_2C_{30}N_{18}H_{24}O$ and $Ni_2C_{30}N_{15}H_{26}O_6Cl$ stoichiometries for compounds **1** and **2**, respectively. Found (Calc.%) for **1**: C, 47.0 (46.87); H, 3.4 (3.15); N, 32.6 (32.82); Ni, 15.4 (15.09). Found (Calc.%) for **2**: C, 42.6 (42.70); H, 2.9 (3.11); Ni, 13.9 (13.74); Cl 4.2 (4.15).

Physical measurements

Infrared spectroscopy was performed on a Perkin-Elmer spectrophotometer in the 250–4000 cm^{-1} region. Magnetic susceptibilities of powdered samples were measured in the 1.8–300 K temperature range using a Quantum Design Squid magnetometer, equipped with a helium continuous-flow cryostat. The magnetic field was approximately 1000 G (0.1 T), at which the *M vs. H* curve is linear even at 1.8 K. The experimental susceptibilities were corrected for the diamagnetism of the constituent atoms (Pascal tables).

Crystal structure determination

X-Ray measurements for compounds **1** and **2** were taken at room temperature on an Enraf-Nonius CAD-4 diffractometer with graphite-monochromated Mo-Kα radiation ($\lambda = 0.71073$ Å), operating in ω–2θ scanning mode using suitable crystals for data collection. Accurate lattice parameters were determined from least-squares refinement of 25 well centred reflections. Intensity data were collected in the θ range 1–30°. During data collection, two standard reflections periodically observed showed no significant variation. Corrections for Lorentz-polarization factors were applied to the intensity values but no absorption corrections were made.

The structures were solved by heavy-atom Patterson methods using the program SHELXS 86[16] and refined by a full-matrix least-squares procedure on F^2 using SHELXL 93.[17] Non-hydrogen atomic scattering factors were taken from ref. 18. Crystallographic data and processing parameters for compounds **1** and **2** are shown in Table 1.

CCDC reference number 186/1566.

See http://www.rsc.org/suppdata/dt/1999/2971/ for crystallographic files in .cif format.

Results and discussion

Structural analysis

The structure of complex **1** consists of centrosymmetric neutral dimers in which the nickel(II) ions are bridged by two end-on azide groups. The co-ordination polyhedra around each metal ion can be described as a NiN_6 distorted octahedron in which three of the N atoms correspond to a terpy ligand and the rest to three azide groups (two end-on and a terminal one). The tridentate terpy and one of the end-on azides occupy the equatorial positions, while the second end-on azide and the terminal azide are in the axial ones (Fig. 1). The end-on azides are located upwards and downwards from the bridge plane, respectively. The terminal azides are in relative *trans* position, each being practically perpendicular to the end-on azide corresponding to the other symmetric unit. There is also a crystallization molecule of water per dimeric unit.

Table 1 Crystal data and structure refinement for compounds **1** and **2**

	1	**2**
Formula	$C_{15}H_{12}N_9NiO_{0.5}$	$C_{30}H_{26}ClN_{15}Ni_2O_6$
M	385.05	845.53
Crystal system	Monoclinic	Triclinic
Space group	$C2/c$	$P\bar{1}$
a/Å	20.979(3)	10.179(2)
b/Å	7.733(1)	10.800(1)
c/Å	20.177(4)	16.866(2)
α/°	—	85.54(2)
β/°	90.29(2)	74.49(2)
γ/°	—	72.03(1)
U/Å^3	3263.6(9)	1728.0(4)
Z	8	2
T/°C	25	25
μ/cm^{-1}	12.12	12.35
Unique data	2433	10050
Observed data	2415	10050
$R(R')$	0.0675(0.1891)	0.0492(0.1276)

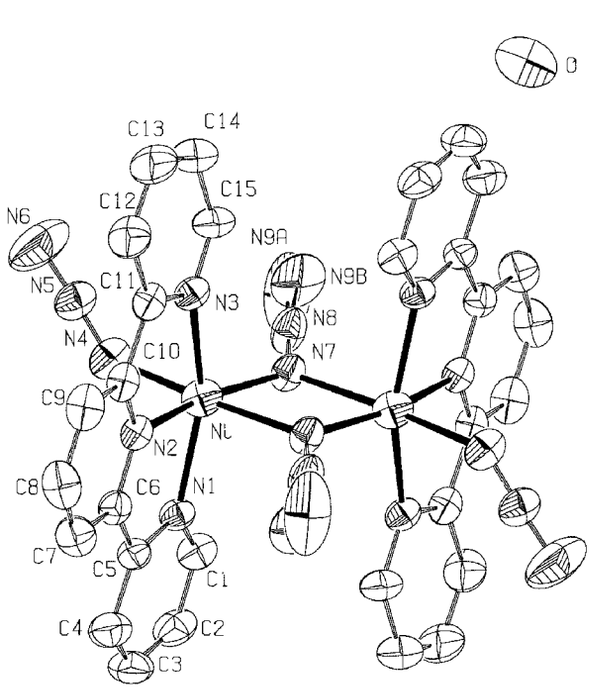

Fig. 1 An ORTEP[19] view (50% probability) of the dimeric unit for compound **1**. The position of the N9 atom of the end-on azide has been split in two (A and B with multiplicities of 0.5) for a better structural resolution.

Table 2 summarises the most relevant structural features for compound **1**. Table 2 also shows some selected parameters for $[\{Ni(terpy)(N_3)_2\}_2]\cdot 2H_2O$ **3**, for comparison. The crystal structure and magnetic properties for **3** are reported elsewhere.[3a] Thus, the structural parameters corresponding to both compounds indicate that the dimeric units in **1** and **3** are very similar. The difference in the number of crystallization molecules of water gives rise to a different crystallographic packing. Compound **3** crystallises in the monoclinic system, space group $P2_1/a$ with the following cell parameters: $a = 15.628(3)$, $b = 9.798(2)$, $c = 10.332(2)$ Å, $\beta = 92.32(2)°$, $Z = 2$.

As can be seen in Table 2 for compound **1**, the bridge between metallic cations shows two different distances (Ni–N(7) and Ni–N(7i) 2.039(3) and 2.184(3) Å, respectively), the Ni–N7–Ni(i) bridge-angle being 101.6(1)°. The distance between

Table 2 Selected bond distances (Å) and angles (°) for compounds **1** and **3**

	1	**3**
Ni–N(1)	2.098(3)	2.081(8)
Ni–N(2)	1.998(3)	1.966(8)
Ni–N(3)	2.113(3)	2.101(8)
Ni–N(4)	2.095(3)	2.071(8)
Ni–N(7)	2.039(3)	2.038(8)
Ni–N(7i)	2.184(3)	2.198(8)
N(4)–N(5)	1.156(5)	1.20(1)
N(5)–N(6)	1.146(6)	1.16(2)
N(7)–N(8)	1.168(5)	1.22(1)
N(8)–N(9)	1.22(4)	1.16(1)
N(2)–Ni–N(1)	78.1(1)	77.6(3)
N(2)–Ni–N(3)	78.2(1)	78.8(3)
N(7)–Ni–N(3)	103.3(1)	103.3(3)
N(1)–Ni–N(7)	100.6(1)	100.3(3)
N(4)–Ni–N(1)	90.8(1)	89.5(3)
N(2)–Ni–N(4)	96.9(1)	98.4(3)
N(4)–Ni–N(3)	88.4(1)	91.2(3)
N(7)–Ni–N(4)	95.4(1)	95.1(3)
N(1)–Ni–N(7i)	90.6(1)	90.5(3)
N(2)–Ni–N(7i)	89.4(1)	87.7(3)
N(3)–Ni–N(7i)	92.8(1)	91.3(3)
N(7)–Ni–N(7i)	78.4(1)	78.7(3)
N(4)–Ni–N(7i)	173.8(1)	171.2(1)
N(6)–N(5)–N(4)	177.6(6)	177(1)
N(7)–N(8)–N(9)	172.2(2)	176(1)
N(5)–N(4)–Ni	124.7(3)	118.4(7)
N(8)–N(7)–Ni	131.0(3)	126.0(7)
N(8i)–Ni(7i)–Ni	124.2(3)	118.6(6)
Ni–N(7)–Ni(i)	101.6(1)	101.3(1)

Symmetry code: (i) $-x+\frac{3}{2}, -y+\frac{3}{2}, -z+1$.

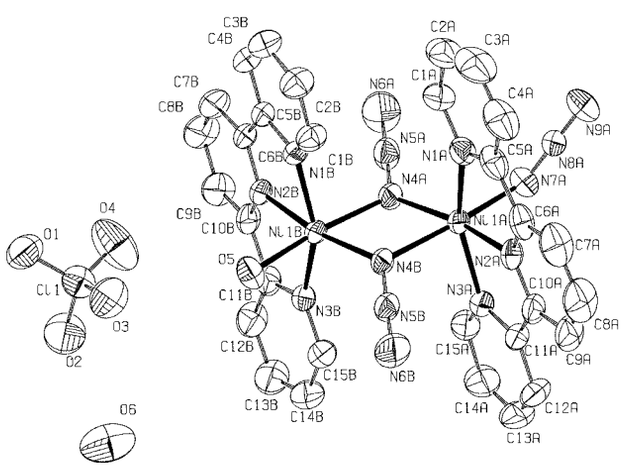

Fig. 2 An ORTEP view (50% probability) of the dimeric unit for compound **2**.

metallic cations and terminal azides is intermediate between the $Ni–N_{end\text{-}on\ azide}$ distances (Ni–N4 2.095(3) Å). The two end-on azides form angles of about 20° with the bridge plane. The similarity between dimeric complexes **1** and **3** is well illustrated by the Ni–N(7) and Ni–N(7i) distances, and the Ni–N7–Ni(i) bridge angle corresponding to **3** (2.038(8) and 2.198(8) Å, and 101.3(1)° respectively).

The octahedral polyhedra can be described assuming that the N_{terpy} and the $N(7)_{end\text{-}on}$ atoms occupy the equatorial positions while the $N(4)_{terminal}$ and $N(7i)_{end\text{-}on}$ atoms are located in the axial ones. Thus, the co-ordination sphere around Ni is not only distorted by the double bridge but also by the tridentate terpy ligands (N_{terpy}–Ni–N_{terpy} angle is 78.15° on average and the Ni–N_{terpy} distances range from 1.998(3) to 2.113(1) Å). Additionally, while N_{terpy} atoms are quasi planar, the N(7) atom is shifted by ≈10° off the equatorial plane.

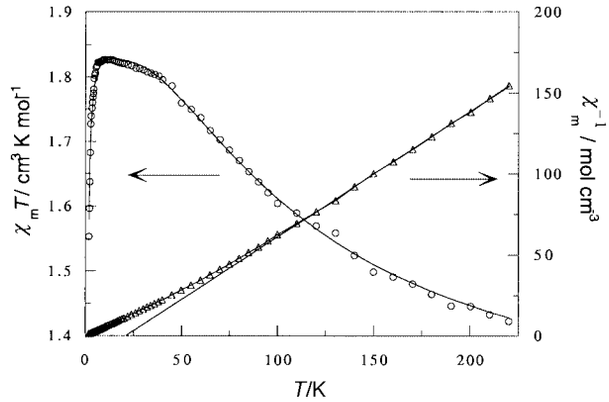

Fig. 3 Thermal evolution of χ_m^{-1} and $\chi_m T$ for compound **1** and their corresponding theoretical curves.

The structure of compound **2**, shown in Fig. 2, differs from that of **1** in the presence of a co-ordinated molecule of water in place of one of the terminal azides **1**. Consequently, the dimeric units for **2** are cationic being accompanied by a ClO_4^- counter anion. Additionally, a crystallization molecule of water can be seen in the asymmetric unit. In Table 3, selected structural parameters for compound **2** can be seen. As for **1**, two different $Ni–N_{end\text{-}on}$ distances can be found for each Ni atom (Ni(1A)–N(4A) and Ni(1B)–N(4B) 2.069(2) and 2.068(2), Ni(1A)–N(4B) and Ni(1B)–N(4A) distances are 2.175(2) and 2.119(2) Å) and an intermediate $Ni–N_{terminal}$ distance (Ni(1A)–N(7A) 2.097(2) Å). The bridge angles (Ni(1A)–N(4A)–Ni(1B) and Ni(1B)–N(4B)–Ni(1A) are 102.5(1) and 100.60(9)°, respectively) are very similar to the one found for compound **1**.

IR spectroscopy

A summary of the most important IR bands corresponding to compounds **1** and **2** together with their tentative assignment is given in Table 4. The major interest of the IR spectra of both compounds is the bands corresponding to the azide groups. Compound **1** shows two intense IR absorptions at 2050 and 2020 cm^{-1} which can be assigned to the ν_{asym} stretch of the terminal and end-on azide ligands, respectively. Similarly, two distinguishable bands could be expected for the azide symmetric stretching mode, ν_{sym}, but only a weak signal at about 1300 cm^{-1} is observed. This can be attributed to the fact that this region is obscured by the terpyridine characteristic bands. Additionally, a split signal corresponding to the azide bending vibration, δ, can also be observed at about 610 cm^{-1}. The IR spectrum of **1** also exhibits a broad signal at 3500 cm^{-1} which can be associated to the crystallization molecule of water.

For compound **2** a broad absorption at 2060 cm^{-1} has been attributed to the ν_{asym} mode of both types of azide groups. Additionally, the ν_{sym} and δ modes of this pseudohalide appear at 1355 and 600 cm^{-1}, respectively. As for **1**, ν_{sym} is a weak absorption which is not split. Two bands at 1100 and 625 cm^{-1} have been attributed to the ν_3 and ν_4 absorptions of the ClO_4^- counter anion. Finally, bands at 1700 and 3590 cm^{-1} corresponding to the coordination and crystallization molecules of water, respectively, have also been observed.

Magnetic properties

The thermal variation of the inverse of the magnetic susceptibility (χ_m^{-1}) and the $\chi_m T$ product are shown in Figs. 3 and 4 for compounds **1** and **2**, respectively. As can be seen in both figures, the Curie–Weiss law is just followed in the high-temperature range for which values of $C_m = 1.27$ (**1**) and 1.23 cm^3 K mol^{-1} (**2**) and $\theta = 23.3$ (**1**) and 20.5 K (**2**) have been calculated along with g values of 2.25 (**1**) and 2.22 (**2**). In both cases the $\chi_m T$ product increases with decreasing temperature, reaching a maximum after which it rapidly decreases. The maxima are

Table 3 Selected bond distances (Å) and angles (°) for compound **2**

Ni(1A)–N(1A)	2.103(2)	N(2A)–Ni(1A)–N(1A)	78.43(10)	N(2B)–Ni(1B)–O(5)	96.53(10)
Ni(1A)–N(2A)	2.003(2)	N(2A)–Ni(1A)–N(3A)	78.06(10)	O(5)–Ni(1B)–N(3B)	154.72(9)
Ni(1A)–N(3A)	2.102(2)	N(4A)–Ni(1A)–N(3A)	101.63(10)	N(4B)–Ni(1B)–O(5)	92.71(10)
Ni(1A)–N(4A)	2.069(2)	N(4A)–Ni(1A)–N(1A)	102.12(10)	N(1B)–Ni(1B)–N(4A)	93.69(9)
Ni(1A)–N(7A)	2.097(2)	N(7A)–Ni(1A)–N(1A)	90.11(10)	N(2B)–Ni(1B)–N(4A)	91.69(9)
Ni(1A)–N(4B)	2.175(2)	N(2A)–Ni(1A)–N(7A)	97.09(10)	N(4A)–Ni(1B)–N(3B)	93.16(9)
Ni(1B)–N(1B)	2.108(2)	N(7A)–Ni(1A)–N(3A)	89.28(10)	N(4B)–Ni(1B)–N(4A)	79.07(9)
Ni(1B)–N(2B)	2.013(2)	N(4A)–Ni(1A)–N(7A)	94.25(10)	O(5)–Ni(1B)–N(4A)	171.78(9)
Ni(1B)–N(3B)	2.122(2)	N(1A)–Ni(1A)–N(4B)	93.62(9)	Ni(1A)–N(4A)–Ni(1B)	102.46(10)
Ni(1B)–N(4B)	2.068(2)	N(2A)–Ni(1A)–N(4B)	90.85(9)	Ni(1B)–N(4B)–Ni(1A)	100.60(9)
Ni(1B)–N(4A)	2.119(2)	N(3A)–Ni(1A)–N(4B)	90.25(9)	N(6A)–N(5A)–N(4A)	177.6(4)
Ni(1B)–O(5)	2.080(2)	N(4A)–Ni(1A)–N(4B)	77.80(9)	N(9A)–N(8A)–N(7A)	179.4(3)
N(4A)–N(5A)	1.188(3)	N(7A)–Ni(1A)–N(4B)	171.76(9)	N(6B)–N(5B)–N(4B)	178.1(3)
N(5A)–N(6A)	1.150(4)	N(2B)–Ni(1B)–N(1B)	77.66(9)	N(5A)–N(4A)–Ni(1A)	129.2(2)
N(7A)–N(8A)	1.177(3)	N(2B)–Ni(1B)–N(3B)	77.84(9)	N(5A)–N(4A)–Ni(1B)	121.1(2)
N(8A)–N(9A)	1.142(4)	N(4B)–Ni(1B)–N(3B)	106.52(9)	N(8A)–N(7A)–Ni(1A)	123.2(2)
N(4B)–N(5B)	1.192(3)	N(4B)–Ni(1B)–N(1B)	98.67(9)	N(5B)–N(4B)–Ni(1B)	129.4(2)
N(5B)–N(6B)	1.146(4)	O(5)–Ni(1B)–N(1B)	87.86(10)	N(5B)–N(4B)–Ni(1A)	120.6(2)

Table 4 Characteristic bands (cm^{-1}) in the IR spectra of compounds **1** and **2** together with the tentative assignments

Complex	$\nu_{asym}(N_3)$	$\nu_{sym}(N_3)$	$\delta(N_3)$	$\nu_3(ClO_4^-)$	$\nu_4(ClO_4^-)$	H_2O_{crys}	H_2O_{coor}
1	2020, 2050i	1300m	610w (s)	—	—	3500 (br)	—
2	2060i (br)	1355m	600w	1100m (br)	625m	3590 (br)	1700w

i = Intense, m = medium, w = weak, br = broad, s = split.

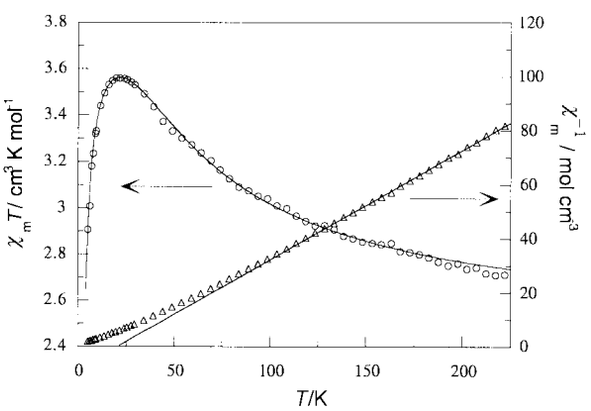

Fig. 4 Thermal evolution of χ_m^{-1} and $\chi_m T$ for compound **2** and their corresponding theoretical curves.

located at 11 and 20 K, for compounds **1** and **2**, respectively. This behaviour indicates the existence of ferromagnetic coupling between metallic centres which has been associated to the end-on azide bridges and a large nickel(II) single-ion zero-field splitting.

For the theoretical analysis of the magnetic behaviour of compounds **1** and **2** the analytical expression developed by Ginsberg *et al.*[20] was used. This is based upon the Hamiltonian (1) where the nickel(II) ion is assumed to be magnetically

$$H = -2JS_1S_2 - D(S_{1z}^2 + S_{2z}^2) - g\beta H(S_1 + S_2) - Z'J'S\langle S\rangle \quad (1)$$

isotropic; J is the usual intradimer exchange parameter, D the zero-field-splitting term of the $^3A_2$ ground state, and $Z'J'$ is the intermolecular magnetic exchange, treated in the molecular field approximation. The best fit using the Ginsberg equation was obtained with values of $J = 22.8$ cm^{-1}, $D = -6.9$ cm^{-1}, $Z'J' = 0.06$ cm^{-1} and $g = 2.20$ (compound **1**) and $J = 13.6$ cm^{-1}, $D = -19.2$ cm^{-1}, $Z'J' = 0.03$ cm^{-1} and $g = 2.12$ (**2**) per Ni atom. Both theoretical curves can also be seen in Figs. 3 and 4. It is worth mentioning that the Ginsberg equation provides accurate values of J and g, while the values of D and $Z'J'$ are less accurate. However, the effects of the latter parameters are most important in the low temperature region where the experimental uncertainties are greatest.

The excellent agreement between the experimental and calculated data for both compounds must be interpreted in terms of an increasing population of the $S = 2$ ground state with decreasing temperature and the subsequent increasing values of $\chi_m T$. At lower temperatures, the single-ion zero-field splitting causes a depopulation into a diamagnetic ground state which accounts for the decreasing of $\chi_m T$ values.

Comparison between magnetic data for compound **1** and its polymorphous **3** reveals, as expected, a similar magnetic behaviour. Thus, as reported,[3a] the ferromagnetic performance of **3** is also described by the Ginsberg equation with values of J, D, $Z'J'$ and g of 20.1 cm^{-1}, −12.5 cm^{-1}, 0.38 cm^{-1} and 2.26, respectively.

Theoretical approach to di-μ-(1,1)-N_3-bridged nickel(II) dimers

Several studies have been carried out so far in order to analyse the influence on the exchange constant J of several structural parameters. In relation to the di-μ-(1,1)-N_3-bridged metal(II) dimers the M–N–M bridge angle (θ) and the M–N distance have been observed to be the most significant parameters. Alvarez and co-workers[14] have recently found parabolic J–θ curves for Cu^{II}. This relationship is related by these authors to the variation of the square of the energy gap between the SOMOs (Δ^2) built up from $d_{x^2-y^2}$ metallic orbitals with θ. Thus, similar J–θ curves were found for Ni^{II}, the calculations being based on hybrid density functional methods.

From an experimental point of view, the attempts made so far to correlate J and the bridge angle for end-on azide-bridged nickel(II) dimers have been rather frustrating since, as can be seen in Fig. 5, all the dimers characterized so far, including the present compounds, exhibit bridge angles over a narrow range of θ (101–105°). On the other hand, from a theoretical point of view, the approach to the nickel(II) dimers is obviously more difficult since two SOMOs must be considered (built up from $d_{x^2-y^2}$ and d_{z^2} metallic orbitals).

In this work, a theoretical approach to di-μ-(1,1)-N_3-bridged nickel(II)-dimers has been done through Extended Hückel Molecular Orbital (EHMO) calculations. The structural model concerns two octahedral spheres connected through (1,1)-N_3 ligands at two of the equatorial positions, the rest of the

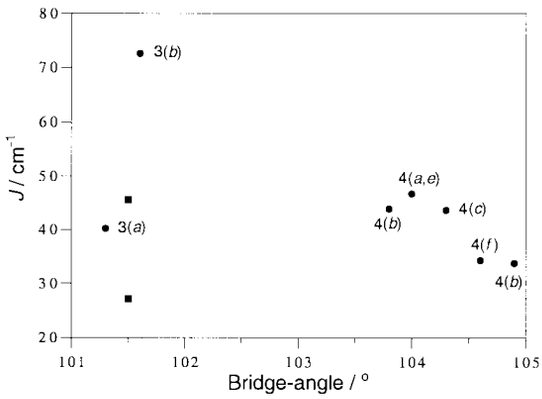

Fig. 5 Experimental J values (unified considering a spin Hamiltonian based on J) *versus* the Ni–N–Ni bridge angle for di-μ-(1,1)-N_3-bridged nickel(II) dimers. The squares correspond to this work, the circles to work reported elsewhere (reference numbers are shown).

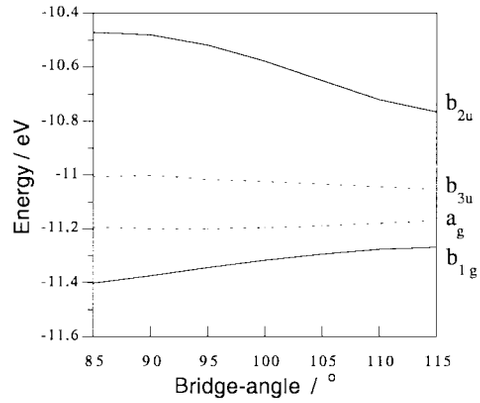

Fig. 6 Walsh diagram for the model di-μ-(1,1)-N_3-bridged nickel(II) dimer showing the energy of the SOMOs built up from $d_{x^2-y^2}$ and d_{z^2} orbitals upon variation of the Ni–N–Ni bridge angle.

co-ordination sites being occupied by NH_3 groups. Chart 1 shows an xy projection of this structural model (NH_3 groups are omitted). The variation in energy with bridge angle (θ) of the molecular orbitals has been estimated by means of the CACAO program.[21] According to the resulting Walsh diagram, the total energy is minimum for values of $\theta = 103°$, rapidly increasing for both lower and higher values of θ. Since these theoretical results quite accurately predict the experimental evidence about the narrow range over which di-μ-(1,1)-N_3-bridged nickel(II) dimers crystallize, it is concluded that the structural model used in this work is quantitatively representative of this type of compound.

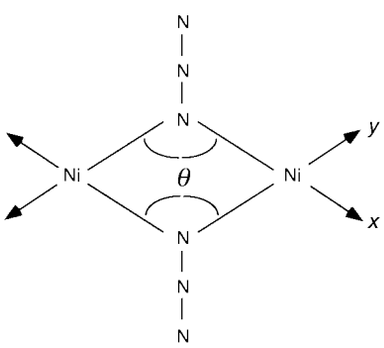

Chart 1

As the authors are aware, no J-Δ^2 correlation has been established for nickel(II) dimers so far. Thus, even though representative experimental data are not available for the study of the influence of Δ^2 (through the variation in the bridge angle) on the magnetic behaviour of di-μ-(1,1)-N_3-bridged nickel(II) dimers, the current theoretical approach also concerns this aspect. Therefore, special attention has been focused on the SOMOs built up from the "magnetic orbitals" $d_{x^2-y^2}$ and d_{z^2}. The energy change with θ of these molecular orbitals can be seen in Fig. 6. Thus, the b_{1g} MO (which corresponds to the symmetric combination of $d_{x^2-y^2}$) is slightly Ni–N_{azide} bonding (Chart 2) and becomes less stable with increasing θ. On the contrary, b_{2u} (which corresponds to the antisymmetric combination of $d_{x^2-y^2}$) is a slightly Ni–N_{azide} antibonding MO (Chart 2) which stabilizes with increasing θ. The symmetric and antisymmetric combinations of d_{z^2} give rise to the a_g and b_{3u} MOs, respectively. Both are of a non-bonding Ni–N_{azide} character, their change in energy with θ being significantly less important.

According to the qualitative approach by Hay *et al.*[22] for nickel(II) dimers, the antiferromagnetic contribution of the

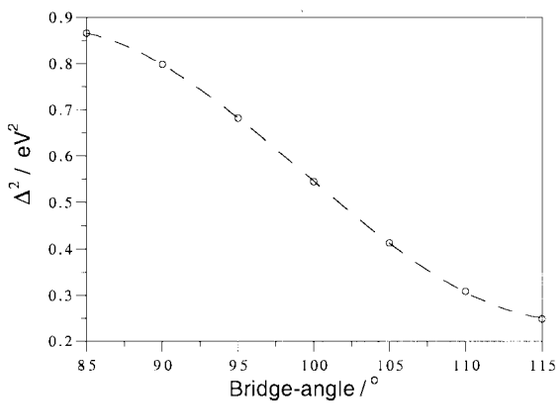

Fig. 7 Variation of the square of the gap between the SOMO built up from $d_{x^2-y^2}$ atomic orbitals with Ni–N–Ni bridge angle for di-μ-(1,1)-N_3-bridged nickel(II) dimers.

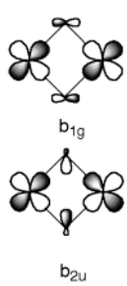

Chart 2

exchange constant, J, is proportional to the square of the energy gap (Δ^2) between the SOMOs built up from both $d_{x^2-y^2}$ and d_{z^2} orbitals. However, Fig. 6 clearly indicates that b_{1g} and b_{2u} (built up from $d_{x^2-y^2}$ orbitals) are the most relevant MOs for the study of the magnetic behaviour of di-μ-(1,1)-N_3-bridged nickel(II) dimers. Thus, in Fig. 7, the square of the energy gap (Δ^2) between b_{1g} and b_{2u} has been plotted against the bridge angle. As can be seen, Δ^2 decreases for increasing bridge angle. As mentioned above, these data should be interpreted as an increasing global exchange constant, J, over the mentioned angle range.

Finally, it should be pointed out that Alvarez and co-workers[14] have established a quantitative correlation between J and θ using the same di-μ-(1,1)-N_3-bridged nickel(II) dimeric model as in the current work. Our results qualitatively agree with their conclusions drawn, but a small disparity can be observed for the angle at which the maximum ferromagnetic exchange constant can be expected (115° for the current work and 105° for Alvarez and co-workers). We acknowledge that

our theoretical calculations are less accurate and admit the higher reliability of the hybrid density functional methods.

Concluding remarks

Two new ferromagnetic end-on azide bridged nickel(II) dimers have been magnetostructurally characterized, both structural and magnetic parameters lying within the typical values for similar nickel(II) dimers. Extended Hückel molecular orbital calculations revealed that the most stable structure corresponds to a value of the Ni–N–Ni bridge angle of 103°. Additionally, the variation of the square of the gap between the SOMOs built up from the $d_{x^2-y^2}$ and d_{z^2} metallic orbitals indicated that the antiferromagnetic contribution of the global coupling constant decreases for increasing Ni–N–Ni bridge angle between 83 and 115°.

Acknowledgements

This work has been carried out with the financial support of the Universidad del País Vasco/Euskal Herriko Unibertsitatea (Grant UPV 130310-EB201/1998), the Gobierno Vasco/Eusko Jaurlaritza (Project PI96/39) and the Ministerio de Educación y Cultura (Project PB97-0637).

References

1 J. Comarmond, P. Plumeré, J. M. Lehn, Y. Agnus, R. Louis, R. Weiss, O. Kahn and I. Morgenstern-Badarau, *J. Am. Chem. Soc.*, 1982, **104**, 6330.
2 S. Sirakov, I. Bkouche-Vaksman and O. Kahn, *Inorg. Chem.*, 1984, **23**, 490.
3 (*a*) M. I. Arriortua, R. Cortés, L. Lezama, T. Rojo, X. Solans and M. Font-Bardia, *Inorg. Chim. Acta*, 1990, **174,** 263; (*b*) R. Cortés, J. I. R. Larramendi, L. Lezama, T. Rojo, K. Urtiaga and M. I. Arriortua, *J. Chem. Soc.*, *Dalton Trans.*, 1992, 2723; (*c*) R. Cortés, L. Lezama, J. I. R. Larramendi, M. Insausti, J. V. Folgado, G. Madariaga and T. Rojo, *J. Chem. Soc.*, *Dalton Trans.*, 1994, 2573; (*d*) R. Cortés, L. Lezama, J. L. Pizarro, M. I. Arriortua and T. Rojo, *Angew. Chem.*, *Int. Ed. Engl.*, 1994, **33**, 2488; (*e*) R. Cortés, J. L. Pizarro, L. Lezama, M. I. Arriortua and T. Rojo, *Inorg. Chem.*, 1994, **33**, 2697; (*f*) R. Cortés, M. K. Urtiaga, L. Lezama, J. L. Pizarro, A. Goñi, M. I. Arriortua and T. Rojo, *Inorg. Chem.*, 1994, **33**, 4009; (*g*) R. Cortés, M. Drillon, X. Solans, L. Lezama and T. Rojo, *Inorg. Chem.*, 1997, **36**, 677; (*h*) R. Cortés, M. K. Urtiaga, L. Lezama, J. L. Pizarro, M. I. Arriortua and T. Rojo, *Inorg. Chem.*, 1997, **36**, 5016.
4 (*a*) A. Escuer, R. Vicente and J. Ribas, *J. Magn. Magn. Mater.*, 1992, **110**, 181; (*b*) R. Vicente, A. Escuer, J. Ribas, M. S. El Fallah, X. Solans and M. Font-Bardia, *Inorg. Chem.*, 1993, **32**, 1920; (*c*) J. Ribas, M. Montfort, C. Díaz, C. Bastos and X. Solans, *Inorg. Chem.*, 1994, **33**, 484; (*d*) J. Ribas, M. Monfort, B. K. Gosh and X. Solans, *Angew. Chem.*, *Int. Ed. Engl.*, 1994, **33**, 2087; (*e*) A. Escuer, R. Vicente, J. Ribas and X. Solans, *Inorg. Chem.*, 1995, **34**, 1793; (*f*) A. Escuer, R. Vicente, M. S. El Fallah, X. Solans and M. Font-Bardía, *Inorg. Chim. Acta*, 1996, **247**, 85; (*g*) A. Escuer, R. Vicente, M. A. S. Goher and F. A. Mautner, *Inorg. Chem.*, 1996, **35**, 6386; (*h*) M. Monfort, J. Ribas, X. Solans and M. Font-Bardía, *Inorg. Chem.*, 1996, **35**, 7366; (*i*) A. Escuer, R. Vicente, M. A. S. Goher and F. Mautner, *Inorg. Chem.*, 1998, **37**, 782.
5 (*a*) S. S. Tandon, L. K. Thompson, M. E. Manuel and J. N. Bridson, *Inorg. Chem.*, 1994, 33, 5555; (*b*) L. K. Thompson, S. S. Tandon and M. E. Manuel, *Inorg. Chem.* 1995, 34, 2356; (*c*) L. K. Thompson and S. S. Tandon, *Comments Inorg. Chem.*, 1996, **18**, 125.
6 G. A. van Albada, M. T. Lakin, N. Veldman, A. L. Spek and J. Reedijk, *Inorg. Chem.*, 1995, **34**, 4910.
7 G. De Munno, T. Poerio, G. Viau, M. Julve and F. Lloret, *Angew. Chem.*, *Int. Ed. Engl.*, 1997, **36**, 1459.
8 T. M. Rajendiran, C. Mathonière, S. Golhen, L. Ouahab and O. Kahn, *Inorg. Chem.*, 1998, **37**, 2651.
9 C.-C. Wang, W.-C. Lo, C.-C. Chou, G.-H. Lee, J.-M. Chen and S.-M. Peng, *Inorg. Chem.*, 1998, **37**, 4059.
10 M. A. Aebersold, B. Gillon, O. Plantevin, L. Pardi, O. Kahn, P. Bergerat, I. von Seggern, F. Tuczek, L. Öhrström, A. Grand and E. Lelièvre-Berna, *J. Am. Chem. Soc.*, 1998, **120**, 5238.
11 O. Kahn, *Inorg. Chim Acta*, 1982, **62**, 3.
12 M. F. Charlot, O. Kahn, M. Chaillet and C. J. Larrieu, *J. Am. Chem. Soc.*, 1986, **108**, 2574.
13 J. Ribas, M. Monfort, R. Costa and X. Solans, *Inorg. Chem.*, 1993, **32**, 695.
14 E. Ruiz, J. Cano, S. Alvarez and P. Alemany, *J. Am. Chem. Soc.*, 1998, **120**, 11122.
15 R. Cortés, M. I. Arriortua, T. Rojo, X. Solans, C. Miravitlles and D. Beltrán, *Acta Crystallogr.*, *Sect. C*, 1985, **41**, 1733.
16 G. M. Sheldrick, SHELXS 86, Program for the Solution of Crystal Structures, University of Göttingen, 1985.
17 G. M. Sheldrick, SHELXL 93, Program for the Refinement of Crystal Structures, University of Göttingen, 1993.
18 *International Tables for X-ray Crystallography*, Kynoch Press, Birmingham, 1974, vol. IV.
19 C. K. Johnson, ORTEP II, Report ORNL-5138, Oak Ridge National Laboratory, Oak Ridge, TN, 1976.
20 A. P. Ginsberg, R. L. Martin, R. W. Brookes and R. C. Sherwwod, *Inorg. Chem.*, **1972**, 11, 2884.
21 C. Mealli and D. M. Proserpio, Computer Aided Composition of Atomic Orbitals (CACAO), 1992; see also, *J. Chem. Educ.*, 1990, **67**, 399.
22 P. J. Hay, J. C. Thibeault and R. J. Hoffmann, *J. Am. Chem. Soc.*, 1975, **97**, 4884.

Paper 9/03558C